Tc interaction with crystalline rock from Äspö (Sweden): Effect of in-situ rock redox capacity

Florian Mathias Huber, Yury Totskiy, Remi Marsac, Dieter Schild, Ivan
Pidchenko, Tonya Vitova, Stepan Kalmykov, Horst Geckeis, Thorsten Schäfer

HAL Id: insu-01715154

https://insu.hal.science/insu-01715154

Submitted on 22 Feb 2018

Accepted Manuscript

Tc interaction with crystalline rock from Äspö (Sweden): Effect of in-situ rock redox capacity

Florian Mathias Huber, Yury Totskiy, Rémi Marsac, Dieter Schild, Ivan Pidchenko, Tonya Vitova, Stepan Kalmykov, Horst Geckeis, Thorsten Schäfer

Please cite this article as: Huber, F.M., Totskiy, Y., Marsac, R., Schild, D., Pidchenko, I., Vitova, T., Kalmykov, S., Geckeis, H., Schäfer, T., Tc interaction with crystalline rock from Äspö (Sweden): Effect of in-situ rock redox capacity, *Applied Geochemistry* (2017), doi: 10.1016/j.apgeochem.2017.01.026.

Tc interaction with crystalline rock from Äspö (Sweden):
Effect of in-situ rock redox capacity

Huber, Florian Mathias[1][*], Totskiy, Yury[1], Marsac, Rémi[1], Schild, Dieter[1], Pidchenko, Ivan[1], Vitova, Tonya[1], Kalmykov, Stepan[2], Geckeis, Horst[1], Schäfer, Thorsten[1]

[1] *Karlsruhe Institute of Technology (KIT), Institute for Nuclear Waste Disposal (INE), P.O. Box 3640, D-76021 Karlsruhe, Germany.*
[2] *Lomonosov Moscow State University (MSU), Department of Chemistry, Leninskie Gory 1-3, 119991, Moscow, Russia*

*corresponding author: florian.huber@kit.edu

Karlsruhe Institute of Technology (KIT)
Institute for Nuclear Waste Disposal (INE)
Hermann-von-Helmholtz-Platz 1
76344 Eggenstein-Leopoldshafen
Germany
Phone: +49 721 60 82 2384
Fax: +49 721 60 82 3927

27

Abstract

29

30 The interaction of Tc(VII) with crushed crystalline rock (Äspö diorite; 1-2 mm size fraction)

31 from the Äspö Hard Rock Laboratory (HRL) (Sweden) was studied by laboratory batch

32 sorption and desorption experiments under Ar atmosphere using both natural and synthetic

33 groundwater. The Äspö diorite used in the experiments was drilled, transported and handled

34 as far as possible under anoxic conditions to preserve the in-situ rock redox capacity. For

35 comparison, identical experiments using artificially oxidized Äspö diorite have been carried

36 out to examine the effect of in-situ redox capacity on Tc uptake. According to the batch

37 studies, Tc(VII) uptake on the Äspö diorite is strongly dependent on redox capacity. Uptake

38 on un-oxidized rock is approximately 2 times higher compared to oxidized rock samples,

39 most likely due to higher Fe(II) contents of the un-oxidized rock. Tc redox states and

40 speciation both on the mineral surface and in the bulk were studied using X-ray

41 photoelectron spectroscopy (XPS) and Tc K-edge X-ray absorption near edge structure

42 (XANES) spectroscopy. The spectroscopic results verify a Tc(VII) reduction to Tc(IV) at the

43 rock surface. Distribution coefficients (K_d) and surface normalized distribution coefficients

44 (K_a) were determined and compared to available literature data. The formation of a Tc

45 colloidal phase was not observed under the geochemical conditions prevailing in the

46 experimental studies. Desorption of Tc is very low under anoxic conditions, but after artificial

47 oxidation Tc mobility is strongly increased. The results of this work clearly highlight the effect

48 of in-situ rock redox capacity on Tc retention.

49

1. Introduction

The generally accepted concept of spent nuclear fuel (SNF) and high-level nuclear waste (HLW) long-term storage is by disposal in deep geological formations at depths of around 250 – 1000 meters (IAEA, 2001). The repository host rock as part of a multi-barrier system plays an important role as retention barrier for radionuclide migration. Thus, the selection of the host rock formation with appropriate geochemical and hydrogeological properties is a key challenge during nuclear waste repository siting and it requires comprehensive scientific research. Crystalline rocks (e.g. granites and gneisses) are considered as potential host rock formations for the deep geological disposal in several countries (e.g. Sweden, Finland, Russia, Korea). The work described herein focuses on crystalline rock samples from the Äspö Hard Rock Laboratory (HRL) (Sweden) which is a generic underground research laboratory (URL) located on the Äspö island near Oskarshamn in southern Sweden dedicated to in-situ studies of processes in crystalline formations concerning deep geological disposal of spent nuclear fuel (SKB, 2011). Radionuclide transport depends strongly on the bedrock hydrogeological and geochemical conditions (pH, Eh, and ionic strength) and is governed by different immobilization-remobilization processes (Grambow, 2008). The most important retention processes to be considered in fractured crystalline rocks are sorption to rock surfaces, redox reactions and matrix diffusion (Bodin et al., 2003; Neretnieks, 1980; Xu and Wörman, 1999).

[99]Tc is one of the main long-lived U and Pu fission products in SNF and is also generated by medical laboratories and research institutions. Because of its relatively high fission yield (*ca.* 6%) and long half-life (2.1×10^5 years) ^{99}Tc is considered as a radioactive component of HLW with significant toxic relevance (Kratz and Lieser, 2013). Technetium mobility in natural systems strongly depends on the redox state. The most stable Tc form under aerobic atmosphere is the pertechnetate ion TcO_4^-, which is very soluble and behaves like a conservative tracer under oxidizing conditions (Rard et al., 1999). In an early work by Bondietti and Francis (1979) using a variety of natural rock materials considerable Tc retention due to reduction of pertechnetate was observed in accordance with Eh/pH

79 conditions. The potential of the TcO_4^-/TcO_2 couple was described with the equation (1)

80 (Meyer and Arnold, 1991):

81
$$E_0(TcO_4^-/TcO_2) = 0.738 - 0.0788 \times pH + 0.0197 \times \log[TcO_4^-]$$
(1)

82 Under aerobic conditions, reported K_d values of Tc on crystalline rocks are negligible,

83 < 1 mL/g in Allard et al. (1979) (contact time 1 day) and < 0.1 − 8.6 mL/g in Videnska and

84 Havlova (2012) (contact time with granitic rocks up to 94 days), whereas under reducing

85 conditions the values are much higher (50 mL/g in (Allard et al., 1979)). Both batch type

86 sorption and column experiments with Hanford sediments (Um and Serne, 2005; Zachara et

87 al., 2007) have revealed that ^{99}Tc is highly mobile and shows virtually no retardation under

88 fully oxidizing conditions. However, under anoxic conditions TcO_4^- is prone to reduction to

89 Tc(IV) and the solubility is limited by the hydrous oxide solid phase $TcO_2 \cdot 1.6H_2O_{(s)}$ (Meyer et

90 al., 1991). As a consequence, distribution coefficients and apparent diffusion coefficients of

91 technetium reported in the literature on natural minerals are scarce and are rarely published

92 together with the respective pe and pH conditions. Tc redox kinetics strongly depend on the

93 availability of reactive Fe(II) in the host rock and the mineral association and speciation on

94 surface (surface complexed, precipitated, and ion exchangeable) (Fredrickson et al., 2009;

95 Heald et al., 2007; Jaisi et al., 2009; Peretyazhko et al., 2008a; Peretyazhko et al., 2008b;

96 Zachara et al., 2007). Äspö *in-situ* and laboratory migration studies (CHEMLAB-2) using Äspö

97 derived natural groundwater revealed ≈1% Tc recovery (after 254 days) of the injected

98 Tc(VII) mass (Kienzler et al., 2003; Kienzler et al., 2009). Batch type studies done in parallel

99 revealed surface normalized distribution coefficients, K_a, values of ≈2.1×10^{-3} m for ^{99}Tc

100 ($t_{contact}$ = 14 d), whereas altered material showed significantly lower values. These results

101 revealed contact/residence time dependent retardation and/or reduction processes. In all

102 studies mentioned above, though carried out under e.g. Ar atmosphere in glove boxes,

103 crystalline rock material used were exposed for a considerable time to air before the

104 experiment. This circumstance might be one of the most important drawbacks in all batch

105 sorption/desorption studies carried out not only on redox sensitive radionuclides but for

106 redox sensitive heavy metals in general. Due to the drastically increased effort in preserving

107 the natural in-situ rock redox capacity during drilling, transporting and storing of the rock

108 material, almost no studies are available using non-oxidized material. In consequence, the

109 distribution coefficients, sorption and reduction properties and behaviour published in

110 numerous studies could be biased and accompanied with high uncertainties. So far, only one

111 study on U interaction with the same un-oxidized Äspö diorite (ÄD) material (provided by

112 KIT-INE) as used in the present study is available (Schmeide et al., 2014). Therefore, the main

113 motivation of this work is to investigate the effect of in-situ rock redox capacity on

114 technetium sorption behaviour by conducting classical batch experiments using non-oxidized

115 and oxidized rock material, respectively.

116

2. Materials and Methods

2.1. Radionuclides

119 *2.1.1. ^{99}Tc*

120 All Tc batch experiments with Tc concentration $\geq 10^{-9}$ M have been carried out using a ^{99}Tc

121 stock solution (13 mM NaTcO$_4$) produced at the Institute of Hot Chemistry, Nuclear Research

122 Centre (former FZK, now KIT) (Karlsruhe, Germany). The solubility limit of Tc(IV) in a wide

123 range of pH-Eh conditions covering most of the natural systems is about 4.4×10^{-9} M (Duro et

124 al., 2006). The detection limit of low-background liquid scintillation counting (LSC)

125 (Quantulus, PerkinElmer, Inc., LSC cocktail Ultima Gold) for ^{99}Tc measurement is $\approx 10^{-10}$ M.

126 *2.1.2. ^{95m}Tc*

127 For experiments with Tc concentrations lower than 10^{-9} M, ^{95m}Tc with a much shorter half-

128 life (61 day) and a main gamma emission line at 204.1 keV was applied. The isotope was

129 produced by proton irradiation of natural Mo foil (50 μm thickness) containing the natural

130 isotopic composition at ZAG Zyklotron AG (Karlsruhe, Germany). After cooling the foil was

131 transported to the Institute for Nuclear Waste Disposal (KIT-INE) and processed to separate

132 technetium according to the technique of (Boyd et al., 1960). The foil was dissolved in a

133 mixture of concentrated H$_2$SO$_4$ and 30% H$_2$O$_2$ and afterwards was slowly neutralized with

134 saturated NaOH (up to alkaline pH). The obtained alkaline solution was passed through a

135 column filled with the anion exchanger Dowex 1x8 (100-200 mesh particle size) with a total

136   volume ca. 3 mL. The column was washed first with 20 mL 1 M $K_2C_2O_4$ to remove residues of

137   molybdate and after rinsing with 20 mL of MilliQ water pertechnetate was eluted with 30 mL

138   1 M $HClO_4$. The last fraction was collected into 2 mL vials, which were measured with γ-

139   spectrometry and samples with ca. 90% of ^{95m}Tc were combined and neutralized with

140   concentrated NaOH. The purification level was monitored with ICP-MS and γ-spectrometry.

141   The use of another column filled with Teva® Resin (Eichrom Technologies, LLC) prior to

142   Dowex significantly increased chemical purity of Tc. Technetium separation on Teva Resin

143   column was performed from ≈ 1.5 M HNO_3 media and after washing the column with 2 M

144   HNO_3 Tc was eluted with 8 M HNO_3 according to the technique reported by (Tagami and

145   Uchida, 1999). A further separation step on the Dowex column results in the purification

146   from NO_3^-, which may act as undesired oxidizing agent, being absent in natural deep

147   geological anoxic groundwaters. The nitrate concentration was initially controlled with

148   nitrate test strips (Merck) and subsequent ion chromatography (IC) analysis. Detection limit

149   of gamma spectrometric analysis of ^{95m}Tc using a 10 mL vial geometry and a high-purity

150   germanium (HPGe) semiconductor detector was estimated to be ≈ 10^{-14}-10^{-15} M (three hours

151   measurement time) depending on the age of the stock solution.

152   **2.2. Solid materials**

153   *2.2.1. Äspö diorite*

154   Diorite is the dominating rock type in the Äspö area (Kornfält et al., 1997). The general

155   mineralogical characterization of ÄD is presented in Table 1. Fresh Äspö diorite was obtained

156   from a drilling campaign at the Äspö HRL (Sweden) in 2011 within the EU project CP CROCK.

157   Details of the sampling procedure and material characterization were originally published

158   within a CROCK S&T contribution (Schäfer et al., 2012). During the core drilling, special care

159   was taken to minimize the exposure of the solid material to air. Therefore, the drilling

160   procedure was carried out with a double tube technique preserving to the best possible

161   anoxic conditions. Natural Äspö groundwater (Eh_{SHE} ≈ -240mV) permanently bubbled with N_2

162   was used as a drilling fluid. After a short visual inspection (max. 5 min) under tunnel

163   atmosphere the cores were directly transferred into a transparent LD-PE bag, which was

164   evacuated three times (≈ -0.4 bar) and purged with nitrogen gas before

165 **Table 1.** *Petrographic characterization of Äspö diorite (Byegård et al., 1998; Kornfält et al.,*
166 *1997).*

Material	Rock type	Mineralogical composition, %		Structural characteristic
Äspö diorite	Quartz monzodiorite/ granodiorite	Plagioclase,	30-50	Porphyritic, medium-grained
		Quartz,	10-25	
		K-feldspar,	10-30	
		Biotite,	10-25	
		Epidote,	3-15	
		Amphibole (mainly hornblende),	< 10	
		Muscovite, titanite, apatite, fluorite, zircon, magnetite		

167

168 welding. The same procedure was applied with an Al bag for the second confinement to
169 prevent oxidation during transportation to the KIT-INE laboratories (see Figure A.1, bottom).
170 At KIT-INE the cores were stored in a barrel under Ar atmosphere ($\approx$ 1 bar overpressure).
171 Two Äspö diorite drill cores (borehole KA2368A-01, cores#1.32 and #1.33) were selected for
172 the experiments. Both cores were chosen because of their (maximal) distance to the tunnel
173 wall (13.04 – 13.52 m (core #1.32) and 13.52 – 14.00 m (core #1.33)) and their petrological
174 characterization (fresh Äspö diorite) during the drilling campaign (Figure A.1, top and
175 middle). For preparation of the crushed material, the cores were transferred into an Ar
176 glovebox equipped with a circular diamond saw and cut into small discs (0.5-1 cm in width).
177 These discs were then manually crushed with a hammer and separated into several size
178 fractions by sieving. For the sorption experiments the 1-2 mm size fraction in diameter was
179 chosen. The N_2-BET surface area of 0.16 m^2/g was measured for this size fraction. This un-
180 oxidized crushed material was stored permanently in the glovebox under Ar atmosphere ($\leq$ 1
181 ppm O_2). Part of this crushed diorite material was exposed to air for one week for artificial
182 surface oxidation to investigate the influence of sample preservation and preparation on Tc
183 uptake. The chemical composition of the rock material used was determined at the Institute

184 for Geosciences, Johannes Gutenberg University (Mainz, Germany) by X-Ray fluorescence

185 (XRF) spectrometry (spectrometer MagiXPRO, Philips) with a Rh anode operated at 3.2 kW).

186 In Table A.1 the XRF data for the material studied is compared to the oxidized Äspö diorite

187 used by Huber et al. (2012) and Huber et al. (2010) and to material from (Byegård et al.,

188 1998). A typical granodiorite composition (Nockolds, 1954) is also added in Table A.1 for

189 comparison. The general composition of the ÄD is typical of granitic rocks with high amount

190 of SiO_2 and Al_2O_3 (quartz and feldspar) (Nockolds, 1954). The Fe^{2+} content of the solid phases

191 was measured by cerimetric titration (cerate oximetry) with potentiometric end point

192 determination (Close et al., 1966). The new un-oxidized ÄD shows a much higher amount of

193 ferrous iron (≈39% Fe^{2+}/Fe_{tot} vs. ≈27% in old ÄD samples) compared to the old oxidized ÄD.

194 This result gives confidence in the approach carried out to preserve the in-situ rock redox

195 capacity. In the work from (Byegård et al., 1998) no information on Fe(II) compounds were

196 reported. In order to estimate the cation exchangeable Fe(II) amount on the mineral

197 surfaces of the Äspö diorite, a method proposed by Heron et al. (1994) was applied using

198 10 mL 1 M $CaCl_2$ (pH = 7) in contact with 2 g of granite for 24 h. Afterwards, an aliquot was

199 taken for Fe(II) quantification by the ferrozine technique. The analytical procedure of the

200 ferrozine technique is described in Viollier et al. (2000). Additionally, Fe data on the new un-

201 oxidized and old oxidized ÄD material determined by XRF are given in the Table A.1, showing

202 that the overall Fe(II) redox buffer is drastically reduced for the oxidized samples. The ion-

203 exchangeable Fe(II) fraction for the un-oxidized ÄD was quantified at approx. 4–6 µg/g,

204 whereas for the oxidized samples lower values around 1–3 µg/g for ÄD are obtained. The

205 rather high uncertainty in the measurements is attributed to the natural heterogeneity of

206 the rock material. The content of ion-exchangeable Fe(II) is about three orders of magnitude

207 lower than Fe(II) amount in the bulk obtained by XRF (see Table A1). However, the ratio

208 between Fe(II) content in fresh and oxidized materials of the order of three is similar for

209 both types of measurements.

2.3. Groundwater

211 Different types of groundwater have been used in the experimental program. Besides the

212 natural Äspö groundwater (ÄGW) a synthetic groundwater simulant (ÄGWS) has been

213 prepared to mimic the CROCK drilling site outflow groundwater composition (see Schäfer et

214 al. (2012)). All chemicals used in the preparation of the synthetic groundwater were of

215 analytical grade. Solutions were prepared with deionized Milli-Q water which was stripped

216 with Ar prior to use. ÄGWS has a comparable composition to natural Äspö groundwater

217 sampled *in-situ* from borehole KA3600-F-2 sampled in a Ar pre-flushed 50 L Teflon-coated Al-

218 barrel at the CP-CROCK site (Heck and Schäfer, 2012). Chemical compositions of the ÄGWS

219 used and natural groundwater samples from Äspö and Grimsel (GGW) (glacial melting water

220 analogue with low ionic strength) are presented in Table 2. Relatively high Eh values of

221 ÄGWS and GGW is explained by the low concentration of the redox couples (e.g.

222 Fe(II)/Fe(III)) in the solution, which cannot be measured using a Pt-electrode.

223 **Table 2**. *Overview of the chemical compositions of the synthetic Äspö groundwater simulant (GWS),*

224 *Äspö groundwater and Grimsel groundwater, respectively.*

	synth. Äspö GWS	Synth. Äspö GWS after 122h contact time	Äspö GW (KA-3600-F-2)	Grimsel GW (MI-shear zone)
pH	8.0 ± 0.05	8.0 ± 0.05	7.8 ± 0.05	9.67 ± 0.05
Eh	390 ± 50mV	n.m.	-240 ± 50mV	320 ± 50mV
$[Mg^{2+}]$	104 ± 1.0 mg/L	104.6 mg/L	69.4 mg/L	12.6 µg/L
$[Ca^{2+}]$	1109 ± 94 mg/L	1134 mg/L	1135 mg/L	5.3 µg/L
$[K^+]$	19.35 ± 3.86 mg/L	21.56 mg/L	10.5 mg/L	
$[Li^+]$	2.53 ± 0.04 mg/L	2.50 mg/L	6.0 mg/L	
$[Fe^{2+,3+}]$	n.m.	n.m.	0.2 mg/L	< D.L.
$[Mn^-]$	2.32 ± 3.02µg/L	23.8 µg/L	0.338 mg/L	< D.L.
$[Sr^{2+}]$	19.68 ± 0.29 mg/L	20.14 mg/L	19.9 mg/L	182 µg/L
$[Cs^+]$	<D.L	< D.L		0.79 µg/L
$[La^{3+}]$	n.m.	n.m.		< D.L.
[U]	0.05 ± 0.01 µg/L	1.70 µg/L	0.11 µg/L	0.03 µg/L
[Th]	0.02 ± 0.01 µg/L	0.07 µg/L	< 0.01 µg/L	< 0.01 µg/L
$[Al^{3+}]$	182.8 ± 56.3 µg/L	439.6 µg/L	13.3 µg/L	42.9 µg/L
$[Na^+]$	1929 ± 29 mg/L	1905 mg/L	1894 mg/L	14.7 mg/L
$[Cl^-]$	4749 ± 145 mg/L	4895 mg/L	4999 mg/L	6.7 mg/L
[Si]	n.m.	n.m.	4.7 mg/L	5.6 mg/L
$[SO_4^{2-}]$	409 ± 5.0 mg/L	411.88 mg/L	394.4 mg/L	5.8 mg/L
$[F^-]$	1.97 ± 0.09 mg/L	1.98 mg/L	1.41 mg/L	6.3 mg/L
$[Br^-]$	21.17 ± 0.37 mg/L	20.96 mg/L	23.2 mg/L	
$[NO_3^-]$	n.m.	n.m.	n.m.	< D.L.

| [HCO$_3$]	n.m.	n.m.	n.m.	3.0 mg/L
[B]	306.5 ± 212.5 µg/L	146.1 µg/L	885 µg/L	

225   n.m. – not measured; D.L. – detection limit.

226

227   **2.4. Batch experiments**

228   *2.4.1. Sorption experiments*

229   Before the start of the batch sorption kinetic experiments the crushed material was

230   contacted with relevant groundwater simulant (GWS) for one day and exchanging the water

231   five times. This step was conducted to remove any remaining fines/colloids from the sieving

232   procedure. In case of un-oxidized ÄD the last step was performed with natural ÄGW to

233   establish more realistic conditions. All batch experiments were carried out in 20 mL LSC vials

234   (HDPE, Zinsser©) inside an Ar glovebox with O$_2$ concentrations ≤ 1 ppm at room

235   temperature (20 ± 2° C). The solid-liquid ratio chosen was 2.00g of granitic rock and 8.0mL of

236   groundwater (250 g/L). Sample duplicates were prepared and kept closed during the

237   sorption experiments to prevent oxidation of Fe(II) at the mineral surfaces. All sorption

238   experiments were conducted at pH 8.1 ± 0.05. Tc(VII) concentrations of 1x10^{-5}M, 1x10^{-8}M

239   and 1x10^{-9}M were used in the experiments. For measurement of ^{99}Tc content in the sample

240   supernatant after the desired contact time 1 mL aliquots were taken and added to 10 mL of

241   Ultima Gold LSC cocktail for analysis with LSC. To differentiate between potentially formed

242   colloidal phases (e.g. Tc(IV) eigencolloids) and dissolved species a phase separation by

243   ultracentrifugation (Beckman Optima XL-90, 90,000 rpm, 694,000 × g) for 1 h was applied.

244   Redox potential of selected samples was measured in the Ar glovebox by using a Metrohm

245   (Ag/AgCl, KCl (3 M)) electrode. The measurements were performed directly in the sample

246   without phase separation. The Eh values were recorded every hour and then corrected for

247   the standard hydrogen potential (Eh always denotes corrected Eh$_{SHE}$ in this work). The Eh

248   values were recorded after ca. 1 hour contact time. The redox potential measurements in

249   the sorption experiments samples were carried out after about two weeks and 1 month

250   contact time, respectively. Every sample was measured over a period of one day in the open

251   vial in the Ar glovebox (< 1 ppm O$_2$) to monitor the Eh evolution. A typical time dependent

252   Eh evolution is shown in Figure 1. The initial drop in Eh is likely due to the equilibration of

253   the electrode with the solution, whereas the continuous drift to more oxidizing potentials in

254   the later period might be explained to be a result of oxidation due to traces of oxygen in the

255   Ar glovebox (< 1 ppm O_2) that seems to be enough to compensate the redox capacity of the

256   sample within 24 hours. Therefore, the lowest Eh value detected was used as most

257   representative for the undisturbed rock/water system in the closed vials.
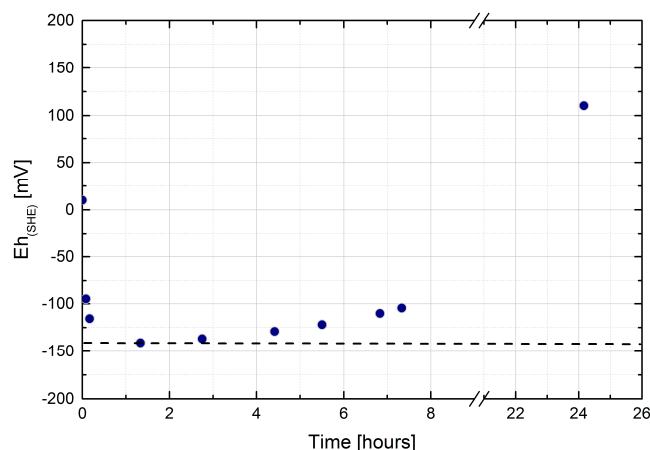
Figure 1: *Typical evolution for Eh measurement in synthetic Äspö groundwater simulant with un-oxidized diorite sample ([Tc] = 10^{-10} M). Dashed line marks the Eh value chosen as the final one.*

258   *2.4.2. Desorption experiments*

259   Subsequent to the sorption kinetic experiments, desorption kinetic studies have been

260   conducted. The Tc containing supernatant of the sorption experiment samples (samples with

261   3 months contact time in the sorption kinetic experiments) was removed and 8 mL of fresh

262   Tc-free groundwater added (natural ÄGW and Grimsel groundwater (glacial meltwater

263   analogue)). For each contact time, the supernatant was always completely removed,

264   analysed by LSC and substituted with fresh Tc-free groundwater of the same volume. A

265   subset of the samples was oxidized under air for one month after the sorption experiments.

266   For this, the initial Tc-containing liquid phase was removed and dry material in the vial was

267   exposed to air before the fresh Tc-free groundwater was added under aerobic atmosphere.

268   For this experiment ÄGWS was used instead of natural ÄGW to keep oxidizing conditions.

269   Desorption experiments cover a time range between a few seconds and 1 month contact

270   time.

271 **2.5. X-ray spectroscopy**

272 *2.5.1. X-ray photoelectron spectroscopy (XPS)*

273 To examine the Tc surface speciation X-ray photoelectron spectroscopy (XPS) was applied.

274 For XPS analysis small un-oxidized Äspö diorite fragments with unpolished faces after cutting

275 by circular saw were contacted with 10^{-5} M Tc(VII) in ÄGWS for two months and washed by

276 MilliQ water for a few seconds to prevent salt precipitation directly before the XPS analysis.

277 All preparation and measurement steps were performed under Ar atmosphere. Transport of

278 the samples from the Ar glovebox to the XPS spectrometer under anoxic atmosphere was

279 achieved by using an O-ring sealed vacuum transfer vessel (PHI model 04-110). XPS

280 measurements were carried out with the XPS system PHI 5000 VersaProbe II (ULVAC-PHI

281 Inc.) equipped with a scanning microprobe X-ray source (monochromatic Al K_α (1486.6 eV) X-

282 rays) in combination with an electron flood gun and a floating ion gun generating low energy

283 electrons (1.1 eV) and low energy argon ions (8 eV) for charge compensation at isolating

284 samples (dual beam technique), respectively. The angle between sample surface and

285 analyser was set to 45°. Survey scans were recorded with an X-ray source power of 12 W and

286 pass energy of 187.85 eV. Narrow scans of the elemental lines were recorded at 23.5 eV pass

287 energy. All spectra were charge referenced to C 1s (hydrocarbon) at 284.8 eV. Data analysis

288 was performed using ULVAC-PHI MultiPak program, version 9.5.

289 *2.5.2. X-ray absorption spectroscopy (XAS)*

290 XAS experiments were performed at the INE-Beamline at the ANKA 2.5 GeV synchrotron

291 radiation facility, Karlsruhe Institute of Technology (KIT), Karlsruhe, Germany. The detailed

292 description of the instrumental setup of the INE-beamline is presented in Rothe et al. (2012).

293 Tc K-edge (21,044 eV) X-ray absorption near edge structure (XANES) spectra were collected

294 in fluorescence mode using one element VITUS Vacuum-Silicon Drift Detector (SDD, Munich,

295 Germany). The uranium mineral meta-schoepite ($UO_3 \cdot nH_2O$) was measured simultaneously

296 with all samples and the Tc(IV) and Tc(VII) references. Pertechnetate solution with

297 concentration of 10^{-2} M was taken as a Tc(VII) reference and $TcO_2 \times 1.6H_2O_{(s)}$ solid phase was

298 prepared by TcO_4^- reduction in the electrochemical cell and used as Tc(IV) reference. The U

299 L_2 (20,948 eV) edge XANES spectra were used for energy calibration. The set of samples with

300 Tc concentrations of ≈10^{-3} M contacted with crystalline rock materials was prepared and

301 mounted in an inert gas cell under argon atmosphere (see Table 3 for an overview of all XAS

302 samples and references measured). During the measurements, argon continually flowed

303 through the cell. Data reduction and normalization was performed with the ATHENA

304 program part of the IFEFFIT software package (Ravel and Newville, 2005).

305 *Table 3.* *List of samples studied by XAS.*

Sample	[Tc], M	Description
Tc(VII) reference	0.01	TcO_4^- solution
Tc(IV) reference	-	Solid TcO_2 covered with supernatant
Tc on ÄD	0.001	Centrifuged suspension

306 **2.6. Thermodynamic modelling**

307 Geochemical speciation calculations and sorption modelling were conducted with the

308 geochemical speciation code PHREEQC (version 2) (Parkhurst and Appelo, 1999). The SIT

309 database provided with PHREEQC is used, in which the thermodynamic constants for Tc

310 correspond to the ones selected by the NEA Thermochemical Database (Guillaumont et al.,

311 2003). Pourbaix diagrams were calculated and plotted with "Geochemist's Workbench"

312 (version 8.0, Aqueous Solution LLC) code with the default database thermo.dat also modified

313 for Tc species in accordance with NEA Thermochemical Database (Guillaumont et al., 2003).

314 Under the applied experimental conditions TcO_4^- and $TcO(OH)_2$ are the only relevant

315 dissolved species for Tc(VII) and Tc(IV), respectively. The redox reaction is:

$$TcO_4^- + 4\,H^+ + 3\,e^- \rightleftharpoons TcO(OH)_2 + H_2O \tag{2}$$
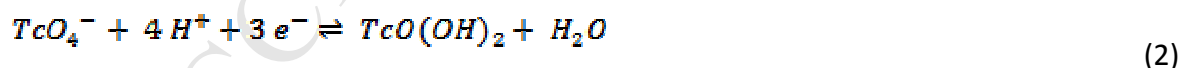
$$K_{VII/IV} = \frac{[TcO(OH)_2]}{[TcO_4^-][H^+]^4[e^-]^3} \tag{3}$$

318 where $K_{VII/IV}$ is the conditional constant of reaction (2) at a given ionic strength. From here

319 the pe (pe = -log a_{e^-} = 16.9×Eh at 25°C) is calculated according to the following equation:

$$pe = \left(\log K_{VII/IV} + \log\left(\frac{[TcO_4^-]}{[TcO(OH)_2]}\right) - 4pH_c\right)/3$$

320

(4)

321 where $pH_c = -\log[H^+]$. The pe corresponding to the 50/50% Tc(VII)/Tc(IV) borderline on a

322 Pourbaix diagram pertaining only to the aqueous species (denoted pe_{aq} or Eh_{aq} for redox

323 potential) is found as follows:

$$pe_{aq} = (\log K_{VII/IV} - 4pH_c)/3$$

324

(5)

325 Sorption of Tc(IV) onto mineral surfaces can also be taken into account. Because this study is

326 restricted to pH ≈8 and low ionic strength for the sorption studies, no surface site protolysis

327 or electrostatics are taken into account. We have considered the following simple reaction

328 (6) to describe sorption onto the mineral surface:

$$\equiv S + TcO_4^- + 4H^+ + 3e^- \rightleftharpoons \equiv STcO(OH)_2 + H_2O$$

329

(6)
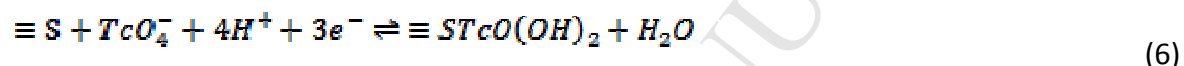
330 where ≡S is a generic surface site and [≡S] can be calculated using equation (7) with the

331 following parameters: site density: 1 site/nm^2; surface area: 0.16 m^2/g; S/V: 250 g/L.

$$[\equiv S] = site\ density \times surface\ area \times (S/V)/N_A = 6.64 \times 10^{-5} mol/L$$

332

(7)

333 where N_A is the Avogadro constant. A similar surface complexation approach was proposed

334 by (Cui and Eriksen, 1996) for Tc uptake by Fe(II)-bearing minerals. According to the reaction

335 (6) the reaction constant is calculated as (8):

$$K_{VII/IV,surf} = \frac{[\equiv STcO(OH)_2]}{[\equiv S][TcO_4^-][H^+]^4[e^-]^3}$$

336

(8)

337 Tc(IV) uptake on mineral surfaces is high (Westsik Jr et al., 2014), so [≡STcO(OH)$_2$] is

338 expected to be much larger than [TcO(OH)$_{2(aq)}$]. By contrast, Tc(VII) uptake on minerals can

339 be neglected (Wildung et al., 2004). Using the surface complexation model, the Tc(VII)/Tc(IV)

340 borderline on a Pourbaix diagram accounting for both processes in solution and at the

341 mineral surfaces (denoted pe_{surf} or Eh_{surf}) is calculated as follows:

342

$$pe = \left(\log K_{VII/IV,surf} + log\left(\frac{[TcO_4^-]}{[\equiv STcO(OH)_2]}\right) - 4pH_c + \log[\equiv S]\right)/3 \qquad (9)$$

343

$$pe_{surf} = \left(\log K_{VII/IV,surf} - 4pH_c + \log[\equiv S]\right)/3 \qquad (10)$$

344　In other words, pe_{surf} is the pe value for 50% Tc uptake. Equation (10) applies only for

345　sufficiently low $[Tc]_{tot}$ or high E_h, i.e. where the precipitation of $TcO_2 \cdot 1.6H_2O_{(s)}$ does not

346　occur. Note that, in a modelling study of plutonium (Pu) uptake on kaolinite, (Marsac et al.,

347　2015a) calculated borderlines between two Pu oxidation states pertaining only to the

348　speciation at the kaolinite surface. Such type of calculation cannot be made in our study

349　because Tc(VII) uptake on minerals is unlikely to be quantifiable, in contrast to the relevant

350　Pu oxidation states.

351　## 3. Results

352　### 3.1. Batch sorption studies

353　*3.1.1. Sorption on Äspö diorite*

354　In the following the term "sorption" implies the total Tc uptake by the solid phase

355　independent of the underlying process (sorption only or reductive sorption). Time

356　dependent sorption of different Tc(VII) concentrations onto oxidized and un-oxidized ÄD are

357　given in Figure 2 for $[Tc]_{tot} = 10^{-5}$ (Figure 2a), 10^{-8} (Figure 2b) and 10^{-9} M (Figure 2c). From the

358　Tc sorption kinetic experiments, it is evident that Tc uptake on un-oxidized material is much

359　higher than the artificially oxidized one. For the sample series of 10^{-8} M and 10^{-9} M $[Tc]_{tot}$ on

360　un-oxidized material plateau values close to 100% sorption are obtained (after 90 days

361　contact time), whereas during the same observation period in experiments with oxidized ÄD

362　only $\approx 40\%$ are removed from solution. Reaching the plateau value for Tc uptake takes more

363　time at lower $[Tc]_{tot}$ concentration. In samples with 10^{-5} M Tc much less relative uptake is

364　observed showing a plateau level for sorbed Tc of around $20 - 25\%$ for the un-oxidized

365　samples and $\approx 10\%$ for the oxidized samples. The steady state is reached after approximately

366　seven days which is much faster than observed for experiments with lower $[Tc]_{tot}$.
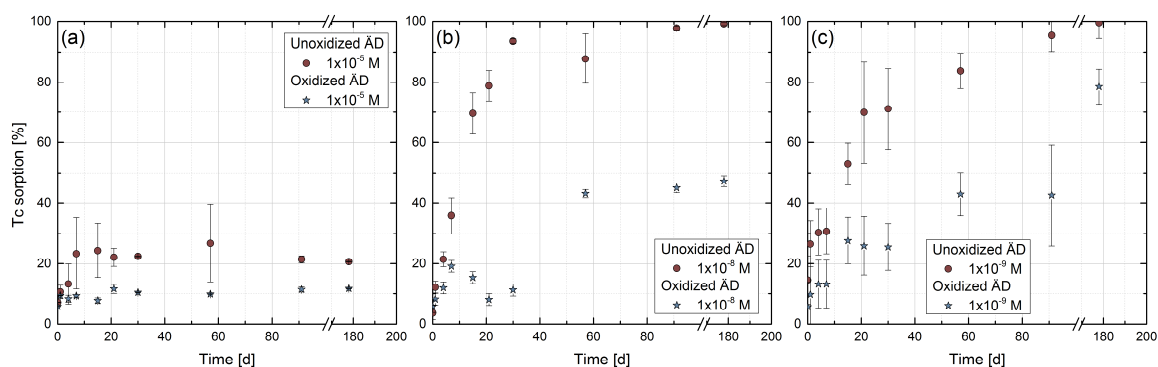
Figure 2. *Tc sorption kinetics for different Tc concentrations in presence of oxidized and un-oxidized ÄD (pH 8, I = 0.2 M).*

367   The formation of colloidal Tc phases (eigencolloids) examined by comparison of Tc

368   concentration in ultracentrifuged to non-ultracentrifuged samples was not detectable within

369   the uncertainty limits (± 5-10%). Either these colloidal phases are not formed or are not

370   stable under the Äspö GWS conditions chosen (ionic strength ≈0.2 M, pH 8).

371   Redox potential measurements of Tc containing ÄGWS after two weeks and 1 month

372   equilibration time with oxidized and un-oxidized ÄD for three different $[Tc]_{tot}$ are shown in

373   Figure 3, together with Pourbaix diagrams calculated for the ÄGW composition. For the

374   oxidized ÄD material the redox potential (Eh_{SHE}) does not change significantly as a function

375   of Tc concentration and is within the range of +230 to +280 mV. However, for un-oxidized

376   ÄD material two trends were observed during the Eh measurements: (a) for low Tc

377   concentration (up to 10^{-8} M) the Eh value decreases with time from 14 days to one month

378   and (b) for the highest Tc concentration used (10^{-5} M) the Eh value was unchanged within

379   the analytical uncertainty. Based on the measured redox potentials in combination with

380   thermodynamic considerations the following conclusions can be drawn (at least after 2

381   weeks contact time): (i) for [Tc] = 10^{-9} M Tc(VII) is reduced to a Tc(IV) species in solution

382   whereas (ii) for [Tc] = 10^{-8} M Tc(IV) precipitates as a solid phase. In case of Tc = 10^{-5} M (iii)

383   Tc(VII) might not be fully reduced to Tc(IV) since the measured Eh_{SHE} values are above the

384   borderline. Nevertheless, a fraction of Tc(VII) might be reduced since the borderline

385   represents already 50%/50% Tc(VIII)/Tc(IV). In this case the reduced Tc precipitates as a

386   Tc(IV) solid phase.
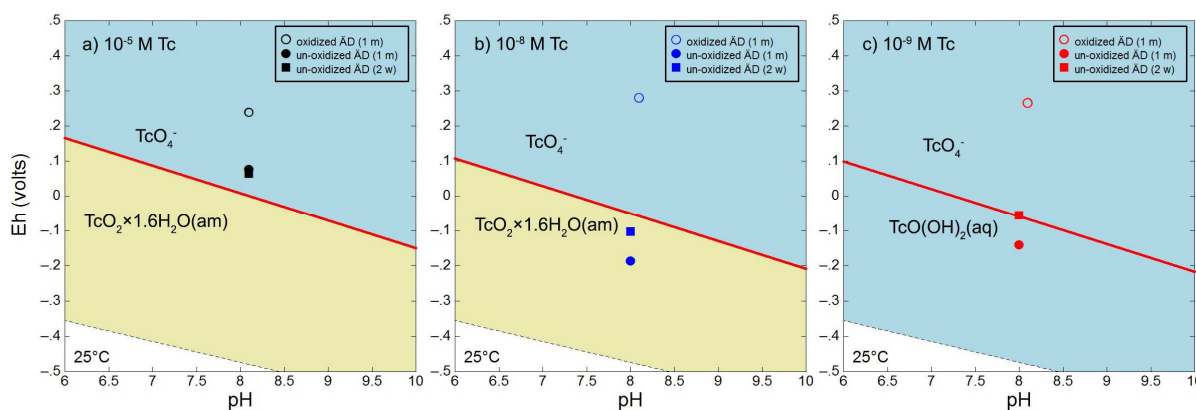
Figure 3. *Pourbaix diagrams for ÄGWS containing different Tc concentrations: (a) 10^{-5} M, (b) 10^{-8} M and (c) 10^{-9} M. Data points are given for oxidized (open symbols) and un-oxidized (filled symbols) ÄD for a contact time of two weeks (squares) and one month (circles).*

3.2. Desorption studies

3.2.1. Desorption experiments without artificial oxidation

Tc desorption was experimentally monitored over one month using sorption samples for which Tc had been previously equilibrated with rock material for three months. Very low Tc desorption was observed in all cases studied irrespective of the nature of the material (oxidized or un-oxidized) used for sorption. For the case of ÄD samples two types of natural groundwater were used, namely Äspö and Grimsel GWs (representing glacial melt water composition with low ionic strength, see Table 2). Tc was detected in the liquid phase only for samples after contact with 10^{-5} M Tc ÄGWS (Figure 4). After 1 day contact time desorption achieved values of up to 7% of the Tc amount sorbed after the uptake studies. This level remained relatively stable up to 30 days of contact time. For lower Tc concentrations (10^{-8} M and 10^{-9} M initial concentration for sorption experiments) no desorption was detected with the detection limit of the analytical method.
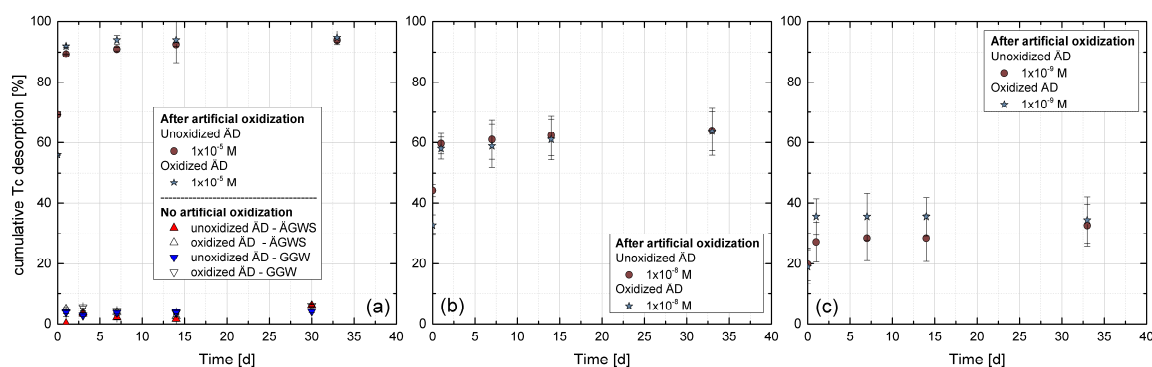
Figure 4. *Desorption of Tc sorbed to oxidized and un-oxidized ÄD material by ÄGWS after 1 month pre-oxidation under atmospheric conditions. Results of the experiment after artificial oxidization and contact with ÄGWS and GGW are additionally included in (a). Please note, that these data points have the unit "% desorbed".*

400 *3.2.2. Desorption experiments with artificial oxidation*

401 Desorption kinetics for ÄD with different $[Tc]_{initial}$ after sample pre-oxidation is given in Figure

402 4. Pre-oxidation of the ÄD samples under aerobic conditions for 1 month before addition of

403 ÄGWS changed the Tc desorption behaviour drastically (Figure 4). Both sorption experiments

404 with originally oxidized and un-oxidized materials revealed the same desorption behaviour.

405 Desorption is fast with the main part of technetium being released after a few seconds

406 contact time and after one day a concentration plateau value was reached.

407 **3.3. Spectroscopic analyses**

408 *3.3.1. X-ray photoelectron spectroscopy (XPS)*

409 XPS analysis of an un-oxidized ÄD disc fragment after contacting with 10^{-5} M Tc(VII) in ÄGWS

410 for2 months under Ar atmosphere in the glovebox revealed that Tc is associated to mafic

411 (dark) minerals only (see Figure A.2), whereas on felsic (light) minerals no Tc was found.

412 Figure 5 (left) shows the measured Tc 3d XPS spectra with the characteristic $3d_{3/2}$ and $3d_{5/2}$

413 peak

17
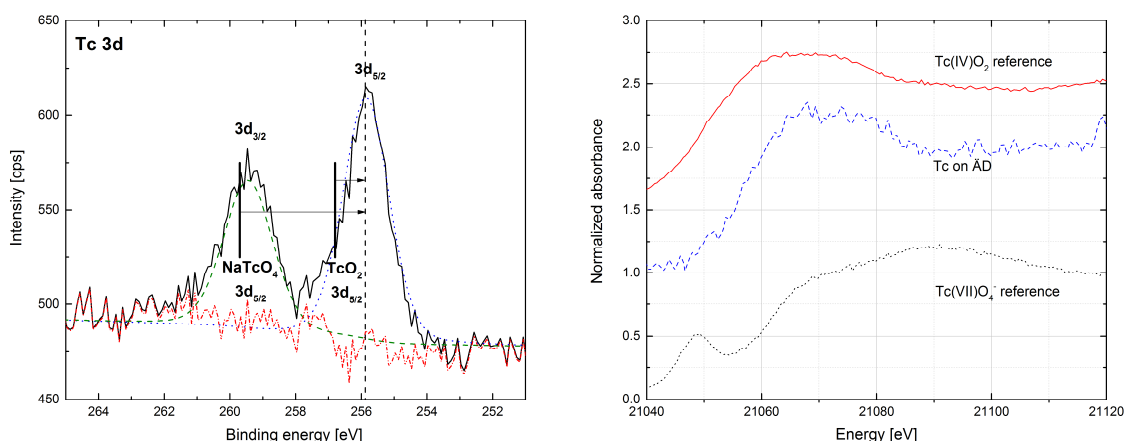
Figure 5. *(left) Tc 3d XPS narrow scan spectrum of an ÄD sample after contacting with Tc(VII)-containing ÄGWS.* The green (dashed) and blue (dotted) curves show the fits to the 3d$_{3/2}$ and 3d$_{5/2}$ XPS elemental lines, respectively, the red line represents the residuum. *(right) Normalized Tc K-edge XANES spectra of a sample after sorption of Tc onto ÄD and of Tc(IV) and Tc(VII) references.*

414   positions. Due to the rather low Tc concentration used in the sorption experiment on the ÄD

415   disc the spectra is quite noisy. Both Tc(VII) and Tc(IV) should have two 3d peaks (3d$_{5/2}$ and

416   3d$_{3/2}$) for each oxidation state. Since there are only two peaks in the area of interest, the

417   conclusion is that there is only one Tc oxidation state present at the mineral surface, and the

418   position of Tc(IV) 3d$_{5/2}$ (TcO$_2$) at 256.8 eV reference line is closer to the experimental data

419   (255.9 eV) than the Tc(VII) 3d$_{5/2}$ (NaTcO$_4$) 259.7 eV reference line. It was therefore

420   concluded that Tc found on the ÄD surface is in the tetravalent oxidation state. Binding

421   energy reference lines for TcO$_2$ and NaTcO$_4$ were taken from (Wester et al., 1987).

3.3.2.   X-ray absorption near-edge structure (XANES)

423   XANES analysis provides bulk information on the Tc oxidation states after interaction of 10^{-3}

424   M Tc with ÄD. Normalized Tc K-edge XANES spectra are presented in Figure 5 (right) for Tc

425   on ÄD together with Tc(IV) and Tc(VII) references. The Tc K-edge XANES spectra of the TcO$_2$

426   and TcO$_4^-$ reference materials have characteristic spectral features, which readily allow Tc

427   oxidation state characterization. For example, the spectrum of the Tc(VII) reference, where

428   Tc is surrounded by four oxygen atoms in tetrahedral conformation, exhibits a pre-edge

429   absorption resonance at about 21,050 eV generated by the 1s → 5p/4d transition (Altmaier

430 et al., 2011b). Since Tc(IV) generally possesses octahedral coordination, this transition is

431 forbidden and the pre-edge feature cannot be seen in the spectrum of the Tc(IV) reference

432 compound. The overall shape and energy position of the rising absorption edge of the Tc K-

433 edge XANES spectrum of Tc on Äspö diorite is similar to the TcO_2 reference without the pre-

434 edge feature of Tc(VII). These fingerprint approach allows to identify Tc(IV) as dominating Tc

435 species on ÄD in line with the XPS results.

4. Discussions

4.1. Tc uptake mechanisms

438 The spectroscopic investigations described above together with the batch

439 sorption/desorption experimental results and the thermodynamic calculations demonstrate

440 that Tc retention in a reducing condition is always coupled to a reduction process from

441 Tc(VII) to Tc(IV). Tc(VII) shows no or only very weak sorption. Thus, the mechanism leading

442 to the removal of Tc from solution may be attributed to (i) a sorption/surface complexation

443 of a Tc(IV) species after reduction in solution by e.g. dissolved Fe(II) and/or (ii) precipitation

444 of poorly soluble $TcO_2 \cdot 1.6H_2O_{(s)}$ again due to Tc(VII) reduction in solution by e.g. dissolved

445 Fe(II) species. Especially in those experiments with the highest Tc concentration a

446 reduction/precipitation process might occur, as the Tc(IV) solubility limit of 4.4×10^{-9} M (Duro

447 et al., 2006) should be significantly exceeded in case of reduction. A third possible

448 mechanism of Tc retention could be (iii) the Tc(VII) reduction by structurally bound or

449 surface bound Fe(II) species. A general scheme of the processes potentially involved into

450 Tc(VII) immobilization is shown in Figure 6.

451 Considering only Fe(II) as a potential reducing agent for Tc(VII)/Tc(IV) the transformation

452 follows according to equation (11):

453
$$TcO_4^- + 3Fe^{2+} + 4H^+ \rightarrow TcO(OH)_2 + 3Fe^{3+} + H_2O \tag{11}$$
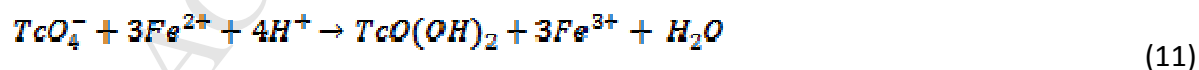
454 In a first attempt we simply tried to assess whether the available amount of Fe(II) is

455 sufficient to reduce added Tc(VII). The ion-exchangeable Fe(II) content was taken as an

456 approximation for the readily "available Fe(II)" and decreases from $(2.2 \pm 0.5) \times 10^{-5}$ M in un-

457 oxidized ÄD to $(9 \pm 5) \times 10^{-6}$ M in oxidized ÄD. Based on the solid to liquid ratio chosen (250

458 g/L) these values give $(1.8\pm0.4)\times10^{-7}$ mol/vial Fe(II) for un-oxidized ÄD and $(7\pm4)\times10^{-8}$

459 mol/vial Fe(II) for oxidized ÄD. Thus, it is obvious that the material extracted and transferred

460 under normal ambient atmospheric conditions (oxidized ÄD) possesses a lower redox

461 capacity. From the comparison of the Fe(II) content $((7\pm4)\times10^{-8}$ mol/vial Fe(II)) with the total

462 amount of added Tc $(8\times10^{-8}$ mol/vial $(10^{-5}$ M Tc), 8×10^{-11} mol/vial $(10^{-8}$ M Tc) and 8×10^{-12}

463 mol/vial $(10^{-9}$ M Tc)) and taking into account that three electrons are required to reduce

464 Tc(VII) to Tc(IV) oxidized ÄD still provides enough ion-exchangeable Fe(II) to reduce

465 $29.1\pm16.7\%$ of total Tc in the sample containing 10^{-5} M Tc, which is close to the experimental

466 observation of $12\pm1\%$ Tc being reduced. Furthermore, un-oxidized ÄD does not provide

467 enough Fe(II) for the complete reduction of 10^{-5} M Tc. These estimations are supported by

468 the finding that Eh values in the granite/water suspensions increase significantly when 10^{-5}
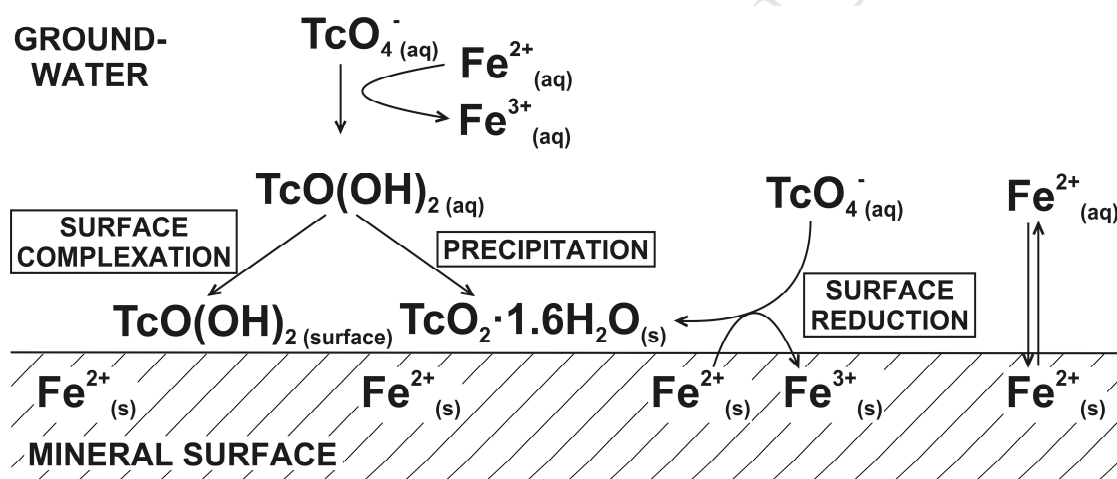
Figure 6. *General scheme of Tc(VII) sorption and reduction processes.*

469 M Tc(VII) are added. This amount is apparently sufficient to exceed the redox capacity of the

470 diorite material at a solid to liquid ratio of 250 g/L. In all batch experiments the granite

471 material should provide enough Fe(II) for the Tc(VII) reduction at lower [Tc]$_{tot}$.

472

4.2. Sorption parameters

474 The temporal change in Tc concentration during the batch sorption experiment can be

475 described with an exponential decay equation (13):

476
$$C_t = (C_0 - C_{eq})e^{-kt} + C_{eq} \qquad (13)$$

477 where C_0 and C_{eq} are the initial and equilibrium Tc concentrations (M), respectively, and k is

478 the sorption rate coefficient (time^{-1}). Hence, calculating sorption S_t as (14)

479
$$S_t = \left(1 - \frac{C_t}{C_0}\right) \times 100\% \qquad (14)$$

480 time dependent sorption data can be fitted with the rate equation (15):

481
$$S_t = S_{eq}(1 - e^{-kt}) \qquad (15)$$

482 where S_t and S_{eq} are the sorption percentages at the moment t and at equilibrium (6 months

483 contact time), respectively. Sorption rate coefficients obtained from this fitting are

484 presented in Table 4. The uptake rates (k) are significantly higher for the experiments with

485 high total Tc concentration, which is a general observation in chemical reaction kinetics. A

486 closer inspection shows that fitting of experimental data obtained with highest Tc

487 concentrations to the kinetic rate model provides a better correlation when two exponential

488 functions (rate constants) are taken. For instance, the sorption of 10^{-5} M Tc onto oxidized ÄD

489 can be fitted with two exponential functions with k values of 0.017±0.008 and 0.265±0.056

490 d^{-1}. This might be an indication of the existence of more than one retention mechanism, e.g.

491 surface sorption and precipitation, respectively. We have to emphasize, however, that the

492 *Table 4. Main parameters obtained by Tc (VII) sorption experiments onto ÄD.*

Mate-rial	Fe(II) available, mg/g	Initial Tc concentration, mol/L	Eh, 1-2 months *, mV	k, d^{-1}	K_d, L/kg	K_a, m	Tc sorbed after 6 months, %
ÄD un-oxi-dized	4-6	1.07×10^{-5}	76	0.24±0.100	1.1±0.200	$(6.80 \pm 0.80) \times 10^{-6}$	21±2.0
		$(1.05 \pm 0.05) \times 10^{-8}$	-187	0.075±0.009	500±200	$(2.90 \pm 1.30) \times 10^{-3}$	99.2±0.6
		$(1.10 \pm 0.10) \times 10^{-9}$	-142	0.036±0.004	900±800	$(5.30 \pm 4.90) \times 10^{-3}$	99.5±6.0
ÄD oxi-	1-3	1.07×10^{-5}	238	0.15±0.040	0.53±0.050	$(3.30 \pm 0.30) \times 10^{-6}$	12±1.0
		$(1.05 \pm 0.05) \times 10^{-8}$	280	0.017±0.010	3.6±1.000	$(2.20 \pm 0.60) \times 10^{-5}$	47±8.0

dized						
	$(1.10\pm0.10)\times10^{-9}$	264	0.007 ±0.001	22±8	$(1.40\pm0.5)\times10^{-4}$	84±6.0

493 * values in Fig. 3; N/A – not applicable.

494

495 system consists of highly coupled redox, precipitation and surface interaction phenomena. A

496 simple interpretation of sorption mechanisms just based on reaction rate analysis is certainly

497 not feasible. This becomes obvious when looking to literature data. Exponential fitting of Tc

498 sorption data from Bondietti and Francis (1979) gives a k value of around 1.1 ± 0.4 d^{-1} for an

499 initial Tc concentration of 1.1×10^{-7} M with Westerly granite as a solid material (167 g/L

500 solid/liquid ratio). The pH/Eh values for this material were also comparable (pH 8, Eh -100

501 mV) to the conditions used in present work, but neither Fe(II) content nor specific surface

502 area of the material were specified in the paper, which could significantly contribute to the

503 enhanced rates found in Bondietti and Francis (1979).

504 Distribution coefficients (K_d in L/kg) obtained for Tc sorption onto Äspö material were

505 calculated using the following equation (16):

$$K_d = \frac{C_l}{C_s} = \frac{A_0 - A_l}{A_l} \times \frac{V}{m_{solid}}$$

506 (16)

507 where C_l and C_s are the equilibrium concentrations of solutes in aqueous and solid phases,

508 respectively, A_0 and A_l are the initial and final aqueous radionuclide activities at equilibrium

509 (Bq/mL), respectively, V is the volume of the aqueous phase (mL) and m_{solid} is the solid

510 mass (g). Typical K_d values obtained within the present work are presented in Table 4

511 together with measured initial Tc concentrations, amount of ion-exchangeable Fe(II) and

512 redox potentials. From a thermodynamic point of view the K_d approach assumes a fully

513 reversible sorption process, but in most papers it is used even when irreversible

514 reduction/precipitation processes are involved (Albinsson et al., 1991; Allard et al., 1979;

515 Kaplan and Serne, 1998). In the report of USEPA (1999) authors describe "conditional" K_d

516 values for the interpretation of experimental data in cases when the rigorous application of

517 the K_d approach is prohibited (e.g. in non-equilibrium, irreversible, or solubility controlled

518 systems). In the present work K_d values are considered as conditional distribution

519   coefficients. For a better comparison of the retention behaviour with literature data, K_d

520   should be normalized to the specific surface area of the solid material used in the

521   experiments according to the equation (17):

$$K_a = \frac{K_d}{S_{BET}} (\times 10^{-6})$$

522   (17)

523   where K_a is the surface area normalized distribution coefficient (m) and S_{BET} is the specific

524   surface area of the solid determined by N_2-BET (m^2/g). K_a values for the ÄD material are

525   shown in Table 4. Since the surface area of oxidized and un-oxidized ÄD remains the same,

526   this normalization does not affect the comparison between them. The K_d values obtained for

527   the oxidized material (see Table 4; 10^{-5} M Tc) in this study with 0.53±0.05 L/kg for oxidized

528   ÄD are in good agreement with recently published data of Videnska and Havlova (2012) who

529   reported a K_d value of 0.3 L/kg under oxidizing conditions for 1.6×10^{-4} M ^{99}Tc on granitic rocks

530   from Melechov Massive, Centre Bohemian Massive, Czech Republic (> 0.8 mm size fraction).

531   Since the surface area was not mentioned in the publication, K_a values cannot be calculated

532   for these results. Batch-type studies on Tc uptake with well-preserved un-oxidized crushed

533   granitic rocks can hardly be found in the literature. We have compared the data obtained

534   with experiments performed under artificial reducing conditions. Ito and Kanno (1988) have

535   published the Tc distribution between solution and granitic rocks (0.49 − 0.83 mm size

536   fraction, 10^{-12} M [^{95m}Tc]) together with a number of other minerals under oxidizing and

537   reducing conditions. Under oxidizing conditions (in 0.16 M $NaNO_3$) K_d values of 0.1 L/kg (K_a =

538   4.8×10^{-7} m) were obtained, while under reducing conditions (0.1 M $NaBH_4$ and 0.16 M

539   $NaNO_3$) values of 45.6 L/kg (K_a = 2.2×10^{-4} m) increasing up to 68 L/kg (K_a = 3.2×10^{-4} m) with

540   decreasing NO_3^- concentration down to 0.016 M could be determined. The paper by

541   McKinley and Scholtis (1993) summarized the data on K_d values of Tc on different materials

542   including granitic rocks used for the safety assessment of waste disposal at that time. Here

543   the values range from 0 to 250 L/kg depending on the experimental conditions and the

544   origin of the rocks. The authors emphasize that Tc sorption under oxidizing conditions is

545   normally very low or zero, and for reducing conditions K_d values increase by 1–2 orders of

546   magnitude.

4.3. Tc desorption

As was shown in the results section, Tc desorption without artificial oxidation of the material is almost negligeable. We suppose that the relatively rapid establishment of a steady state for the Tc concentration after only 1 day desorption is the consequence of washing out residual Tc(VII) in the porewater rather than desorption of sorbed or precipitated Tc(IV). For the desorption experiments after artificial oxidation, the general trend of the fast desorption up to a plateau value might be explained by the rapid oxidation of surface associated Tc(IV) to the heptavalent oxidation state and thus to the (almost) non-sorbing pertechnetate anion whereas strongly sorbing un-oxidized Tc(IV) does not have any significant contribution to the desorption processs. The same observations were made by numerous investigators (Begg et al., 2008; Burke et al., 2006; Morris et al., 2008), where Tc(IV) oxidation to Tc(VII) was found to be a driving force for the Tc desorption process. Taking into account Tc uptake mechanisms discussed in section 4.1, one can assume two different mechanisms, namely predominantly surface complexation for log $[Tc]_{tot}$ = -8 and -9 and $TcO_2 \cdot 1.6 H_2O_{(s)}$ precipitation for log $[Tc]_{tot}$ = -5 governing the Tc sorption process. Consequently, for the same initial Tc concentration, a similar Tc desorption behaviour can be expected for oxidized and un-oxidized systems, which is in a good agreement with the experimental data observed for the ÄD. A higher degree of desorption observed for the samples with higher $[Tc]_{initial}$ might be explained by the relatively easier oxidation of the surface associated $TcO_2 \cdot 1.6 H_2O_{(s)}$ phase in comparison to the surface complexed Tc(IV) species (see Table 5) which are probably more recalcitrant to remobilization during oxidation. Similar presumptions were expressed (Begg et al., 2008; Burke et al., 2006; Morris et al., 2008), but the mechanistical nature of this resistance is still a matter of further research.

Table 5. *Comparison of the sorption/desorption values for the oxidized and un-oxidized ÄD for the artificially oxidized sample series. Desorption time of 1 month.*

| Material	-log $[Tc]_{initial}$	Tc sorption, %	Tc desorption, %
	5	21±2	93.7±0.6
ÄD (un-oxidized)	8	99.2±0.6	64±7
	9	99.5±6	33±7
ÄD (oxidized)	5	12±1	94±3

24

8	47±8	64±8
9	84±6	35±8

4.4. Spectroscopic analyses

According to the XPS results (see Figure 5 left), the Tc signal was detected only on dark mica-type mineral surface (most likely biotite or magnetite), which contains structural Fe(II). It is well known that Tc(VII) is concentrated on Fe(II)-containing minerals (Burke et al., 2010; Fredrickson et al., 2009; McBeth et al., 2011) as "hotspots" due to surface (heterogeneous) reduction into insoluble Tc(IV) oxide phase or/and homogeneous reduction in the solution into soluble Tc(IV) species with subsequent sorption on the mineral surface. According to the results of Peretyazhko et al. (2008a) heterogeneous Tc(VII) reduction on the surface associated Fe(II) is orders of magnitude faster than the homogeneous reduction by aqueous Fe^{2+} and may occur on the Fe(II)-containing mineral surfaces. XANES analysis of the Äspö diorite contacted with Tc-containing ÄGWS indicated the presence of Tc(IV) as well.

4.5. Thermodynamic modelling

The general scheme of the modelling applied is described in Section 2.6. A similar calculation approach was applied in previous studies related to the modelling of Pu sorption to kaolinite (Marsac et al., 2015a) and Np sorption on illite (Marsac et al., 2015b) with respect to the differences in chemistry. Figure 7 shows the Tc(IV) fraction in the aqueous phase modelled with PHREEQC for log $[Tc]_{tot} \leq -8$ as a function of the redox potential. For pH = 8.0 and I = 0.1 M, Eh of the $[Tc(VII)]_{aq}/[Tc(IV)]_{aq}$ borderline is -53 mV (Eh_{aq}, calculated from equation (5)), as highlighted in Figure 7. To account for sorption processes (see equation (9)), log $K_{VII/IV,surf}$ is determined as follows. The site density is arbitrarily set equal to 1 site/nm^2, which is the same order of magnitude as commonly observed for several minerals (Burlakov et al., 2000; Jeppu and Clement, 2012). The value for log $K_{VII/IV,surf}$ is strongly dependent on this arbitrarily chosen site density. At Eh values ≤ -90 mV almost all Tc is calculated to be Tc(IV) (see Figure 8). Such conditions prevail in the experiments with un-oxidized ÄD and log $[Tc]_{tot} \leq -8$. Taking these experimental data, log $K_{VII/IV,surf}$ is deduced by a fitting procedure and is found to be equal to 35.7 (see equation (8)). This value is kept constant for all the following calculations.
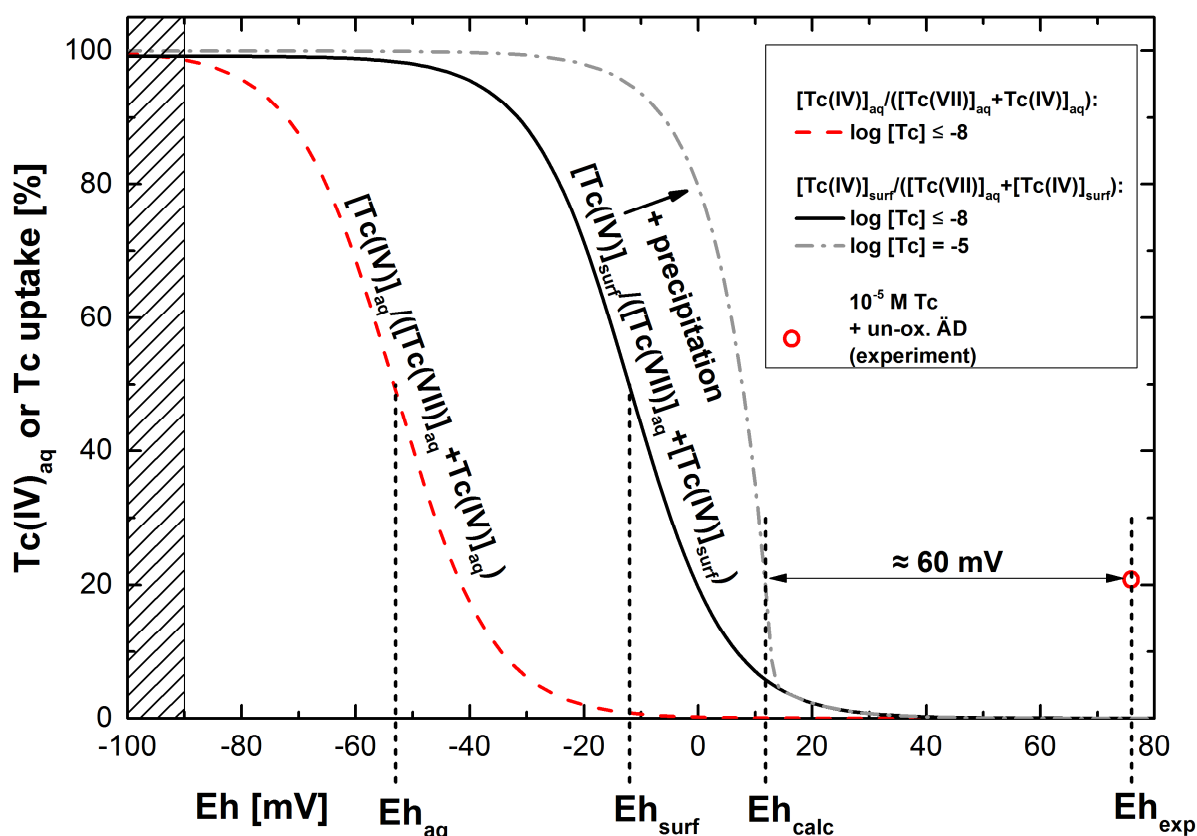
Figure 7. *Tc(IV) fractions depending on the redox potential (pH 8, I = 0.1 M) calculated according to the equations (4) and (9), respectively. Eh_{exp} corresponds to the measured redox potential; Eh_{calc} relates to the calculated redox potential where 21% of Tc is removed from solution in the experiment with log $[Tc]_{tot}$ = -5; $[Tc(VII)]_{aq}/[Tc(IV)]_{aq}$ and $[Tc(VII)]_{aq}/[Tc(IV)]_{surf}$ borderline redox potentials are as well marked by vertical dashed lines; the shaded area at the left side shows the Eh region where model calculations predict quantitative uptake.*

585   The borderline redox potential where $[Tc(IV)]_{surf}$ and $[Tc(VII)]_{aq}$ exist in equimolar

586   concentrations, Eh_{surf}, is found equal to -12 mV in accordance to the equation (10). In

587   agreement with the findings of Marsac et al. (Marsac et al., 2015a; Marsac et al., 2015b) for

588   Np and Pu sorption to clays, the strong sorption behaviour of Tc(IV) shifts the borderline Eh

589   to higher values as compared to that for the $[Tc(IV)]_{aq}/[Tc(VII)]_{aq}$ ratio, Eh_{aq}, in aqueous

590   solution in the absence of mineral surfaces. For log $[Tc]_{tot}$ = -5 precipitation of $TcO_2 \cdot 1.6H_2O_{(s)}$

591   is predicted, which represents the 2nd retention mechanism, and extends the stability field of

592   Tc(IV) further. In the respective experiment the measured Eh value (Eh_{exp}) is 76 mV ± 50mV,

593   where the model predicts insignificant uptake in disagreement with the experimentally

594   observed ≈21% uptake. Actually, the model is very sensitive to the redox potential. For

595   instance, a change in Tc uptake from 2% to 80% is predicted by assuming a slight decrease in

596   Eh_{calc} from +20 to 0 mV for log $[Tc]_{tot}$ = -5. Regarding the uncertainties of experimental Eh

597   data in a range of ±50 mV (Altmaier et al., 2011a) and the incertitude of model parameters,

598   our simulation results are not so different from experimental data. The discrepancy of Tc

599   uptake in simulation and experiment can easily be explained by uncertainties in redox

600   potential measurements. According to model calculations, the dominating uptake

601   mechanism at log $[Tc]_{tot}$ = -5 is precipitation of $TcO_2 \cdot 1.6H_2O_{(s)}$. This is in agreement with

602   XANES measurements performed with a 1 mM Tc-containing solution contacted with the

603   crushed material. The model predicts almost 100% Tc uptake for Eh ≤ -90 mV in accordance

604   with the experimental results for un-oxidized ÄD at log $[Tc]_{tot}$ ≤ -8 (see Table 4). However,

605   relatively high Tc uptake (> 30%, see Table 4 & 5) of the oxidized materials at log $[Tc]_{tot}$ ≤ -8

606   and rather high Eh values (> 200 mV) cannot be explained by the thermodynamic model. No

607   Tc reduction and no uptake is calculated above Eh ≥ ≈30 mV (see Figure 7). Nevertheless, Tc

608   uptake by the oxidized materials is significant but is lower as compared to that by the un-

609   oxidized ÄD (see Figure 2). This finding may suggest that, although oxidized, a redox partner

610   for the reduction of Tc(VII) to Tc(IV) is present in significant amounts, which, however, is not

611   detected by the Eh measurements using a Pt-electrode. Another aspect relates to the

612   concentration of redox partners required for reproducible and thermodynamically defined

613   redox potential measurements using a Pt-electrode, which is proposed to be ≥ ≈10^{-6} M

614   (Grenthe et al., 1992). The ion-exchangeable ferrous iron concentration in the oxidized rock

615   materials lie very close to that minimum value of (9±5)×10^{-6} M Fe(II) for oxidized ÄD. It

616   seems likely that Fe(II) content available is quantitatively consumed during the Tc reduction

617   process by oxidization to Fe(III) inhibiting a precise Eh determination by the platinum

618   electrode. Thus a higher uncertainty in the Eh measurements and in the interpretation of the

619   results needs to be considered for the higher $[Tc]_{tot}$ series and the oxidized ÄD.

620

621   **5. Conclusions**

622

623   A batch type sorption/desorption study on Tc interaction with crushed granitic rock material

624   from the generic URL in Sweden (Äspö HRL) was performed. Part of the crushed material

625   from Äspö HRL used in the experiments has been obtained and handled under anoxic

626   conditions before and during the experiments thus representing to a great extent natural *in-*

627   *situ* rock material conditions (e.g. redox capacity) relevant to the far-field environment of a

628   repository in crystalline rock. According to the experimental findings, Tc(VII) is reduced

629   under natural anoxic conditions to Tc(IV) followed by either precipitation of $TcO_2 \cdot 1.6H_2O_{(s)}$

630   or/and surface complexation of soluble Tc(IV) species on the rock surface. Comparison of

631   samples after ultracentrifugation shows no detectable amount of Tc colloidal phase under

632   simulated groundwater conditions applied. After contact of Tc(VII)-containing groundwater

633   simulants with crystalline rock materials, Tc(IV) species were detected on mafic mica-type

634   Fe-containing minerals. Apparently, the Tc(VII) concentration directly influences the amount

635   of Tc uptake on un-oxidized and oxidized material, which can be correlated with the ion-

636   exchangeable Fe(II) buffer available (4 – 6 µg/g for un-oxidized ÄD and 1 – 3 µg/g for

637   oxidized ÄD). Tc behaviour on oxidized ÄD differs dramatically compared to un-oxidized ÄD

638   samples. In general, artificially oxidized rock material could retain approx. 2 times less Tc

639   compared to un-oxidized material. Distribution coefficients (K_d) and surface area normalized

640   distribution coefficients (K_a) were determined for artificially oxidized and original un-oxidized

641   ÄD which serve as parameters for transport modelling or performance assessment modelling

642   purposes. Technetium desorption from the ÄD is insignificant under anoxic conditions, but

643   after artificial oxidation technetium mobility is increased due to re-oxidation of Tc(IV) to

644   Tc(VII). Such reactions might become relevant in scenarios where oxidized glacial melt water

645   intrusion into a repository is considered. The similar Tc desorption behaviour from the

646   initially oxidized and un-oxidized ÄD samples indicates the same retention mechanism for

647   both types of the material even taking into account the difference in the total uptake

648   capacity. Samples from the batch sorption studies with high $[Tc]_{tot}$ show increased

649   desorption most probably due to faster re-oxidation of the $TcO_2 \cdot 1.6H_2O_{(s)}$ precipitate in

650   comparison to surface complexed Tc(IV) species. According to the thermodynamic

651   calculations, for log [Tc] ≤ -8 Tc(IV) surface complexation is a predominant process of Tc

652   immobilization, while at higher Tc concentration $TcO_2 \cdot 1.6H_2O_{(s)}$ precipitation plays the main

653 role. This work clearly highlights the importance of using well-preserved (un-oxidized)
654 natural materials for the reliable estimation of the interaction of redox sensitive elements
655 with these solid phases. The difference in retention capacity between artificially oxidized and
656 un-oxidized material is highly significant. The data obtained gives important implications on
657 the prediction of Tc behaviour under natural conditions for safety assessment of deep
658 geological disposals of SNF and HLW in undisturbed and disturbed crystalline environments.

6. Acknowledgements

667

668

7. References

670

Albinsson, Y., Christiansensatmark, B., Engkvist, I., Johansson, W., 1991. Transport of actinides and Tc through a bentonite backfill containing small quantities of iron or copper. Radiochim Acta 52-3, 283-286.

Allard, B., Kigatsi, H., Torstenfelt, B., 1979. TECHNETIUM - REDUCTION AND SORPTION IN GRANITIC BEDROCK. Radiochemical and Radioanalytical Letters 37, 223-229.

Altmaier, M., Gaona, X., Fellhauer, D., Buckau, G., 2011a. Intercomparison of redox determination methods on designed and near-natural aqueous systems, FP 7 EURATOM Collaborative Project "Redox Phenomena Controlling Systems". KIT Scientific Publishing.

Altmaier, M., Kienzler, B., Duro, L., Grivé, M., Montoya, V., 2011b. 3rd Annual Workshop Proceedings of the Collaborative Project "Redox Phenomena Controlling Systems" (7th EC FP CP RECOSY). KIT INE.

Begg, J.D.C., Burke, I.T., Charnock, J.M., Morris, K., 2008. Technetium reduction and reoxidation behaviour in Dounreay soils. Radiochim Acta 96, 631-636.

Bodin, J., Delay, F., de Marsily, G., 2003. Solute transport in a single fracture with negligible matrix permeability: 2. mathematical formalism. Hydrogeology Journal 11, 434-454.

Bondietti, E.A., Francis, C.W., 1979. Geologic Migration Potentials of Technetium-99 and Neptunium-237. Science 203, 1337-1340.

Boyd, G.E., Larson, Q.V., Motta, E.E., 1960. Isolation of milligram quantities of long-lived technetium from neutron irradiated molybdenum. J Am Chem Soc 82, 809-815.

Burke, I.T., Boothman, C., Lloyd, J.R., Livens, F.R., Charnock, J.M., McBeth, J.M., Mortimer, R.J.G., Morris, K., 2006. Reoxidation behavior of technetium, iron, and sulfur in Estuarine sediments. Environmental Science & Technology 40, 3529-3535.

Burke, I.T., Livens, F.R., Lloyd, J.R., Brown, A.P., Law, G.T.W., McBeth, J.M., Ellis, B.L., Lawson, R.S., Morris, K., 2010. The fate of technetium in reduced estuarine sediments: Combining direct and indirect analyses. Applied Geochemistry 25, 233-241.

Burlakov, V.M., Sutton, A.P., Briggs, G.A.D., Tsukahara, Y., 2000. Simulation of Porous Si and SiOx Layer Growth, in: MSM (Ed.), Technical Proceedings of the 2000 International Conference on Modeling and Simulation of Microsystems, University of Oxford, UK, pp. 95-97.

Byegård, J., Johansson, H., Skålberg, M., Tullborg, E.-L., 1998. The interaction of sorbing and non-sorbing tracers with different Äspö rock types. Sorption and diffusion experiments in the laboratory scale.

Close, P., Hornyak, E.J., Baak, T., Tillman, J.F., 1966. Potentiometric titration of micro amounts of iron(II) with very dilute cerium(IV) sulfate. Microchemical Journal 10, 334-339.

Cui, D., Eriksen, T.E., 1996. Reduction of Pertechnetate in Solution by Heterogeneous Electron Transfer from Fe(II)-Containing Geological Material. Environmental Science & Technology 30, 2263-2269.

Duro, L., Grivé, M., Cera, E., Gaona, X., Domènech, C., Bruno, J., 2006. Determination and assessment of the concentration limits to be used in SR-Can. SKB.

714 Fredrickson, J.K., Zachara, J.M., Plymale, A.E., Heald, S.M., McKinley, J.P., Kennedy,
715   D.W., Liu, C., Nachimuthu, P., 2009. Oxidative dissolution potential of biogenic and
716   abiogenic TcO2 in subsurface sediments. Geochimica et Cosmochimica Acta 73,
717   2299-2313.
718 Grambow, B., 2008. Mobile fission and activation products in nuclear waste disposal. Journal
719   of Contaminant Hydrology 102, 180-186.
720 Grenthe, I., Stumm, W., Laaksuharju, M., Nilsson, A.C., Wikberg, P., 1992. Redox potentials
721   and redox reactions in deep groundwater systems. Chemical Geology 98, 131-150.
722 Guillaumont, R., Fanghänel, T., Fuger, J., Grenthe, I., Neck, V., Palmer, D.A., Rand, M.H.,
723   2003. Update on the Chemical Thermodynamics of Uranium, Neptunium, Plutonium,
724   Americium and Technetium. Elsevier.
725 Heald, S.M., Zachara, J.M., Jeon, B.H., McKinley, J.P., Kukkadapu, R., Moore, D., 2007.
726   XAFS study of the chemical and structural states of technetium in Fe(III) oxide Co-
727   precipitates. X-Ray Absorption Fine Structure-XAFS13 882, 173-175.
728 Heck, S., Schäfer, T., 2012. Short Note: CP CROCK groundwater sample characterization
729 Heron, G., Crouzet, C., Bourg, A.C.M., Christensen, T.H., 1994. Speciation of Fe(II) and
730   Fe(III) in contaminated aquifer sediments using chemical extraction techniques.
731   Environ. Sci. Technol. 28, 1698-1705.
732 Huber, F., Enzmann, F., Wenka, A., Bouby, M., Dentz, M., Schäfer, T., 2012. Natural micro-
733   scale heterogeneity induced solute and nanoparticle retardation in fractured crystalline
734   rock. Journal of Contaminant Hydrology 133, 40-52.
735 Huber, F., Seher, H., Kunze, P., Bouby, M., Banik, N.L., Hauser, W., Geckeis, H., Kienzler,
736   B., Schäfer, T., 2010. Laboratory study on colloid migration and colloid-radionuclide
737   interaction under Grimsel groundwater conditions simulating glacial melt-water
738   intrusion in the Äspö system. KIT INE.
739 IAEA, 2001. The use of scientific and technical results from underground research laboratory
740   investigations for the geological disposal of radioactive waste. IAEA, Vienna.
741 Ito, K., Kanno, T., 1988. Sorption behavior of carrier-free technetium-95m on minerals, rocks
742   and backfill materials under both oxidizing and reducing conditions. J Nucl Sci
743   Technol 25, 534-539.
744 Jaisi, D.P., Dong, H.L., Plymale, A.E., Fredrickson, J.K., Zachara, J.M., Heald, S., Liu, C.X.,
745   2009. Reduction and long-term immobilization of technetium by Fe(II) associated
746   with clay mineral nontronite. Chemical Geology 264, 127-138.
747 Jeppu, G.P., Clement, T.P., 2012. A modified Langmuir-Freundlich isotherm model for
748   simulating pH-dependent adsorption effects. Journal of Contaminant Hydrology 129–
749   130, 46-53.
750 Kaplan, D.I., Serne, R.J., 1998. Pertechnetate exclusion from sediments. Radiochim Acta 81,
751   117-124.
752 Kienzler, B., Vejmelka, P., Römer, J., Fanghänel, E., Jansson, M., Eriksen, T.E., Wikberg, P.,
753   2003. Swedish-German actinide migration experiment at ÄSPÖ hard rock laboratory.
754   Journal of Contaminant Hydrology 61, 219-233.
755 Kienzler, B., Vejmelka, P., Römer, J., Schild, D., Jansson, M., 2009. Actinide migration in
756   fractures of granite host rock: laboratory and in situ investigations. Nuclear
757   Technology 165, 223-240.
758 Kornfält, K.A., Persson, P.O., Wikman, H., 1997. Granitoids from the Äspö area, southeastern
759   Sweden - geochemical and geochronological data. GFF 119, 109-114.
760 Kratz, J.V., Lieser, K.H., 2013. Nuclear and Radiochemistry: Fundamentals and Applications.
761   Wiley.

762 Marsac, R., Banik, N.L., Lützenkirchen, J., Buda, R.A., Kratz, J.V., Marquardt, C.M., 2015a.
763   Modeling plutonium sorption to kaolinite: Accounting for redox equilibria and the
764   stability of surface species. Chem Geol 400, 1-10.
765 Marsac, R., Banik, N.L., Lutzenkirchen, J., Marquardt, C.M., Dardenne, K., Schild, D., Rothe,
766   J., Diascorn, A., Kupcik, T., Schafer, T., Geckeis, H., 2015b. Neptunium redox
767   speciation at the illite surface. Geochimica et Cosmochimica Acta 152, 39-51.
768 McBeth, J.M., Lloyd, J.R., Law, G.T.W., Livens, F.R., Burke, I.T., Morris, K., 2011. Redox
769   interactions of technetium with iron-bearing minerals. Mineralogical Magazine 75,
770   2419-2430.
771 McKinley, I.G., Scholtis, A., 1993. A comparison of radionuclide sorption databases used in
772   recent performance assessments. Journal of Contaminant Hydrology 13, 347-363.
773 Meyer, R.E., Arnold, W.D., 1991. The Electrode Potential of the Tc(IV)-Tc(VII) Couple,
774   Radiochim. Acta, p. 19.
775 Meyer, R.E., Arnold, W.D., Case, F.I., Okelley, G.D., 1991. Solubilities of Tc(IV) Oxides.
776   Radiochim Acta 55, 11-18.
777 Morris, K., Livens, F.R., Charnock, J.M., Burke, I.T., McBeth, J.M., Begg, J.D.C., Boothman,
778   C., Lloyd, J.R., 2008. An X-ray absorption study of the fate of technetium in reduced
779   and reoxidised sediments and mineral phases. Applied Geochemistry 23, 603-617.
780 Neretnieks, I., 1980. Diffusion in the rock matrix - An important factor in radionuclide
781   retardation. Journal of Geophysical Research 85, 4379-4397.
782 Nockolds, S.R., 1954. Average Chemical Compositions of Some Igneous Rocks. Geol Soc
783   Am Bull 65, 1007-1032.
784 Parkhurst, D.L., Appelo, C.A.J., 1999. User's Guide to PHREEQC (Version 2) - A Computer
785   Program for Speciation, Batch-Reaction, One-Dimensional Transport, and Inverse
786   Geochemical Calculations, p. 312.
787 Peretyazhko, T., Zachara, J.M., Heald, S.M., Jeon, B.H., Kukkadapu, R.K., Liu, C., Moore,
788   D., Resch, C.T., 2008a. Heterogeneous reduction of Tc(VII) by Fe(II) at the solid-
789   water interface. Geochimica Et Cosmochimica Acta 72, 1521-1539.
790 Peretyazhko, T., Zachara, J.M., Heald, S.M., Kukkadapu, R.K., Liu, C., Plymale, A.E., Resch,
791   C.T., 2008b. Reduction of Tc(VII) by Fe(II) sorbed on Al (hydr)oxides.
792   Environmental Science & Technology 42, 5499-5506.
793 Rard, J.A., Rand, M.H., Anderegg, G., Wanner, H., 1999. Chemical Thermodynamics of
794   Technetium. Elsevier.
795 Ravel, B., Newville, M., 2005. ATHENA, ARTEMIS, HEPHAESTUS: data analysis for X-
796   ray absorption spectroscopy using IFEFFIT. J Synchrotron Radiat 12, 537-541.
797 Rothe, J., Butorin, S., Dardenne, K., Denecke, M.A., Kienzler, B., Loble, M., Metz, V.,
798   Seibert, A., Steppert, M., Vitova, T., Walther, C., Geckeis, H., 2012. The INE-
799   Beamline for actinide science at ANKA. Rev Sci Instrum 83.
800 Schäfer, T., Stage, E., Büchner, S., Huber, F., Drake, H., 2012. Characterization of new
801   crystalline material for investigations within CP CROCK. 1st Workshop Proceedings
802   of the Collaborative Project „Crystalline Rock Retention Processes" (7th EC FP CP
803   CROCK), 63-72.
804 Schmeide, K., Gürtler, S., Müller, K., Steudtner, R., Joseph, C., Bok, F., Brendler, V., 2014.
805   Interaction of U(VI) with Äspö diorite: A batch and in situ ATR FT-IR sorption study.
806   Applied Geochemistry 49, 116-125.
807 SKB, 2011. Äspö Hard Rock Laboratory: Annual report.

808 Tagami, K., Uchida, S., 1999. Comparison of the TEVA center dot Spec resin and liquid-
809   liquid extraction methods for the separation of technetium in soil samples. J Radioanal
810   Nucl Ch 239, 643-648.
811 Um, W., Serne, R.J., 2005. Sorption and transport behavior of radionuclides in the proposed
812   low-level radioactive waste disposal facility at the Hanford site, Washington.
813   Radiochim. Acta 93, 57-63.
814 USEPA, 1999. The Kd model, methods of measurement, and application of chemical reaction
815   codes, Understanding variation in partition coefficient, Kd values. United States
816   Environmental Protection Agency, Office of Air and Radiation, p. 212.
817 Videnska, K., Havlova, V., 2012. Retention of Anionic Species on Granite: Influence of
818   Granite Composition, Waste Management 2012, Phoenix, Arizona, USA.
819 Viollier, E., Inglett, P.W., Hunter, K., Roychoudhury, A.N., Van Cappellen, P., 2000. The
820   ferrozine method revisited: Fe(II)/Fe(III) determination in natural waters. Applied
821   Geochemistry 15, 785-790.
822 Wester, D.W., White, D.H., Miller, F.W., Dean, R.T., Schreifels, J.A., Hunt, J.E., 1987.
823   Synthesis and characterization of technetium complexes with phosphorus-containing
824   ligands - the homoleptic trimethylphosphite, dimethylmethylphosphonite and
825   methyldiethylphosphinite technetium(I) cations. Inorg Chim Acta 131, 163-169.
826 Westsik Jr, J.H., Cantrell, K.J., Serne, R.J., Qafoku, N.P., 2014. Technetium Immobilization
827   Forms. Literature Survey.
828 Wildung, R.E., Li, S.W., Murray, C.J., Krupka, K.M., Xie, Y., Hess, N.J., Roden, E.E., 2004.
829   Technetium reduction in sediments of a shallow aquifer exhibiting dissimilatory iron
830   reduction potential. Fems Microbiol Ecol 49, 151-162.
831 Xu, S., Wörman, A., 1999. Implications of sorption kinetics to radionuclide migration in
832   fractured rock. Water Resources Research 35, 3429-3440.
833 Zachara, J.M., Heald, S.M., Jeon, B.-H., Kukkadapu, R.K., Liu, C., McKinley, J.P.,
834   Dohnalkova, A.C., Moore, D.A., 2007. Reduction of pertechnetate [Tc(VII)] by
835   aqueous Fe(II) and the nature of solid phase redox products. Geochimica et
836   Cosmochimica Acta 71, 2137-2157.
837
838
839
840

Supplementary Material

841
842
843

Figure A.1. *(Top and middle) Cores used in the batch experiments directly after drilling. (Bottom) Two-layers packing of the cores, sealed into LD-PE and Al bags.*

844
845
846
847

848 **Table A.1.** *XRF data on Äspö diorite (material used in this study, old oxidized ÄD samples*
849 *used in (Huber et al., 2010 & 2012), oxidized ÄD from (Byegård et al., 1998)), and typical*
850 *granodiorite (Nockolds, 1954) composition.*

Element (RMS$_{rel}$)	Äspö diorite (this study), wt. %	Äspö diorite, (Huber et al., 2010 & 2012), wt. %	Äspö diorite (Byegård et al., 1998), wt. %	Typical granodiorite (Nockolds, 1954), wt. %
SiO_2 (0.4%)	62.71	66.06	60.1	66.88
Al_2O_3 (0.7%)	17.27	16.89	18.1	15.66
Fe_2O_3 (0.8%)	4.39	2.6	5.1	1.33
FeO (0.8%)	2.51	0.87	-	2.59
MnO (1.8%)	0.08	0.05	0.1	0.07
MgO (0.3%)	1.76	0.8	2.2	1.57
CaO (0.5%)	3.75	2.41	4.4	3.56
Na_2O (1.3%)	4.55	4.91	4.7	3.84
K_2O (0.8%)	3.05	4.38	3.2	3.07
TiO_2 (1.0%)	0.66	0.35	0.8	0.57
P_2O_5 (1.1%)	0.24	0.12	0.3	0.21
Loss on ignition (LOI)	0.67	1.37	1.0	0.65
Sum	*99.1*	*99.4*	*100*	*100*

Trace element (LLD)	Concentration, ppm	Concentration, ppm	Concentration, ppm	
Ba (10.5ppm)	1162	n.d.	1770	
Co (2.2ppm)	11	5	n.d.	
Cr (5.3 ppm)	24	6	n.d.	
Cu (1.6 ppm)	2	1	n.d.	
Ga (1 ppm)	23	19	n.d.	
Nb (1.1 ppm)	15	9	n.d.	
Ni (3.7 ppm)	18	6	n.d.	
Pb (2.7 ppm)	17	16	89	

Sc	6	4	n.d.
(2.7 ppm)			
Sr	1052	770	1300
(1.5 ppm)			
Th	9.5	5.7	5.2
(1.7 ppm)			
U	4.4	1.8	2.1
(1.1 ppm)			
V	62	36	n.d.
(6.1 ppm)			
Y	22	16	18.1
(1.3 ppm)			
Zn	76	43	n.d.
(1.1ppm)			
Zr	168	139	256
(0.9ppm)			

851   n.d. – not detected, RMS_{rel} – relative root square mean, LLD – lower limit of detection;
852   RMS_{rel} and LLD are taken from the ÄD XRF analysis.

853

854

855
856
857

858 **Table A.2.** List of samples from the batch sorption studies and long-term sorption
859 experiments on un-oxidized and oxidized ÄD.

Material	Contact time, days	Tc uptake, %													
		log [Tc] = -5		log [Tc] = -6		log [Tc] = -7		log [Tc] = -8		log [Tc] = -9		log [Tc] = -10		log [Tc] = -11	
		%	±. %	%	±. %	%	±. %	%	±. %	%	±. %	%	±. %	%	±. %
un-oxidized ÄD	0.04	7.10	0.06					3.57	2.16	14.51	8.08				
	1	8.38	0.06					13.42	2.00	25.14	7.59				
	1	12.80	0.06					10.82	2.02	27.94	7.59				
	4	19.94	0.06					19.04	1.95	33.15	7.40				
	4	6.47	0.06					23.95	1.89	27.54	7.54				
	7	35.15	0.05					41.64	1.67	35.55	7.33				
	7	11.54	0.06					29.96	1.82	25.95	7.59				
	15	15.37	0.08					76.46	1.15	52.74	6.85				
	15	33.37	0.07					62.74	1.38	53.14	6.83				
	21	25.12	0.08					83.88	1.00	53.14	6.83				
	21	19.14	0.08					73.74	1.20	86.73	5.76				
	30	22.43	0.08					93.48	0.77	71.13	6.28				
	57	13.90	0.09					79.66	1.09	70.35	6.31				
	57	39.59	0.07					95.86	0.70	97.14	5.41				
	91	20.26	0.08					97.56	0.65	96.34	5.43				
	91	22.63	0.08					97.90	0.64	94.34	4.98				
	141	44.76	0.12	48.19	0.19	48.70	0.24	53.83	0.23	90.85	0.51	81.65	1.73	95.06	4.15
	141	46.67	0.12	25.49	0.16	41.41	0.21	85.39	0.40	90.34	0.49	76.36	0.99	95.65	4.66
	178	20.70	0.08					99.44	0.58	100.00	5.12				
	178							98.88	0.60	99.54	5.12				
oxidized ÄD	0.04	5.69	0.09					7.61	2.06	-3.45	8.35				
	0.04							4.02	2.10	8.15	8.06				
	1	9.40	0.09					7.65	2.06	18.96	7.78				
	1	9.31	0.09					8.59	2.05	-5.84	8.39				
	4	7.08	0.09					12.12	2.02	9.76	8.01				
	4	9.45	0.09					11.74	2.02	10.56	7.99				
	7	8.83	0.09					23.04	1.90	5.35	8.11				
	7	9.69	0.09					15.23	1.98	14.95	7.87				
	15	6.75	0.09					14.51	1.99	25.36	7.61				
	15	8.59	0.09					16.21	1.97	24.95	7.61				
	21	13.09	0.09					2.57	2.11	33.35	7.40				
	21	10.08	0.09					13.49	2.00	13.36	7.92				
	30	10.38	0.09					11.23	2.03	22.96	7.68				
	57	9.90	0.09					76.91	1.14	39.35	7.23				
	57	9.82	0.09					43.11	1.66	42.55	7.14				
	91	10.51	0.09					53.55	1.52	23.37	7.66				
	91	12.21	0.09					36.51	1.74	57.77	6.71				
	141	3.07	0.71	13.79	0.15	17.12	0.17	18.52	0.17	77.49	2.29	80.46	2.51	67.14	1.23
	141	1.64	0.09	8.56	0.15	16.69	0.17	16.96	0.17	24.18	1.11	63.70	1.17	60.10	1.02

Mate-rial	Con-tact time. days	Tc uptake. %													
		log [Tc] = -5		log [Tc] = -6		log [Tc] = -7		log [Tc] = -8		log [Tc] = -9		log [Tc] = -10		log [Tc] = -11	
		%	±. %	%	±. %	%	±. %	%	±. %	%	±. %	%	±. %	%	±. %
	178							54.83	1.82	90.15	5.67				
	178	11.69	0.09					39.70	1.82	77.75	6.07				

860
861
862
863

864

Figure A.2. *ÄD sample for XPS after contacting with Tc(VII)-containing ÄGWS. Red circle indicates the region where Tc(IV) was found.*

865
866
867
868
869
870
871
872
873

Paper highlights:

- Tc sorption/desorption kinetics investigation was performed on both oxidized and un-oxidized Äspö diorite (Sweden) on different Tc concentrations.
- The difference between artificially oxidized and well-preserved natural rock material is shown.
- Tc colloidal phase formation was not detected under simulated natural conditions.
- Spectroscopic investigations shown the accumulation of Tc(IV) species on mafic (e.g. mica, magnetite) minerals
- Tc sorption parameters on the rock material studied (distribution coefficient, sorption rate) were derived.